ACS APPLIED MATERIALS & INTERFACES

Research Article

www.acsami.org

Co_3O_4 Nanoparticles with Multi-Enzyme Activities and Their Application in Immunohistochemical Assay

Jinlai Dong,[†] Lina Song,[†] Jun-Jie Yin,[‡] Weiwei He,[‡] Yihang Wu,[†] Ning Gu,*[,†] and Yu Zhang*[,†]

[†]State Key Laboratory of Bioelectronics, Jiangsu Key Laboratory for Biomaterials and Devices, School of Biological Science and Medical Engineering, Southeast University, Nanjing 210096, P.R. China

[‡]Center for Food Safety and Applied Nutrition, Food and Drug Administration, College Park, Maryland 20740, United States

Supporting Information

ABSTRACT: Co_3O_4 nanoparticles (Co_3O_4 NPs), synthesized by the coprecipitation method, showed intrinsic catalase-like, peroxidase-like, and SOD-like activity. The catalytic activity of Co_3O_4 NPs was much higher than analogous Fe_3O_4 NPs. Co_3O_4's mechanisms of catalytic activity were analyzed in detail using the electron spin resonance (ESR) method, which confirmed that Co_3O_4 NPs don't follow the classical Fenton reactions with hydrogen peroxide the way Fe_3O_4 NPs do. The high redox potential of Co^{3+}/Co^{2+} was supposed to be the leading cause of the differences in both activity and mechanism with Fe_3O_4. Based on the high, peroxidase-like activity, a new immunohistochemical assay was designed in which the avastin antibody was conjugated onto the surface of Co_3O_4 NPs. The conjugates obtained were used to detect vascular endothelial growth factor (VEGF) that was overexpressed in tumor tissue. When the experimental and control groups were stained, there were clear distinctions between them. This study showed that there are many opportunities to improve the enzyme-like activities of nanomaterials and also to improve their potential applications for biocatalysis and bioassays, especially in relatively harsh conditions.

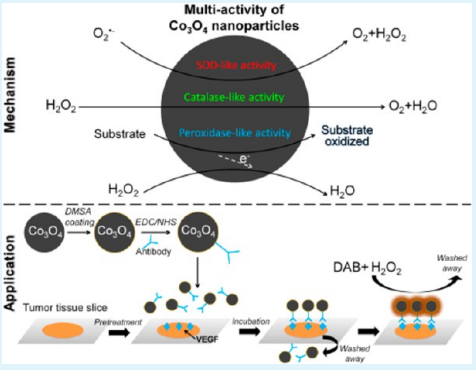

KEYWORDS: *cobalt oxide nanoparticles, multi-enzyme mimetics, high redox potential, immunohistochemical assay*

1. INTRODUCTION

Enzymes are generally proteins that catalyze chemical reactions, and they have an important place in bioassays due to their incredible efficiency and high substrate specificities. However, enzymes can be denatured, are sensitive to environmental factors, and are expensive to produce, limiting their uses and applications.[1−3] Mimic enzymes, which are more stable and can be large-scale synthesized via mature chemical methods at relatively low cost, have attracted intensive attention. Among many candidates, nanomaterials appeared compelling with their high specific surface area and unique shape, composition, and structure properties. Recently, iron oxide nanoparticles (NPs) were found to possess intrinsic peroxidase-like activity and showed potential to replace natural peroxidase in bioassays.[4]

It is common knowledge that high catalytic enzyme activity is often required for high-sensitivity detection in enzyme-linked assays. To improve the catalytic activity of nanoparticle mimic enzymes, numerous strategies such as size control,[5] surface charge regulation,[6] surface modification,[7] and structure control[8] have been studied. Generally, the catalytic activity of NPs increases as particle size is reduced because smaller particles have larger specific surface areas and expose more active sites. Particles that have opposite surface charges to a substrate often display a higher affinity due to electrostatic adsorption. The catalytic activity also depends strongly on the ability of crystal structures to preferentially expose catalytically active atoms. According to Smirnov et al.'s work,[9] the peroxidase-like activity of iron oxide originates mainly from ferrous ions on the surface of NPs. The mechanism may follow Fenton reactions,[10] which can be written as eqs 1 and 2, where k_1 and k_2 are reaction rate constants.

$$Fe^{2+} + H_2O_2 \xrightarrow{k_1} Fe^{3+} + {}^{\bullet}OH + OH^-, \quad k_1 = 76\ L\ mol^{-1}\ s^{-1} \tag{1}$$

$$Fe^{3+} + H_2O_2 \xrightarrow{k_2} Fe^{2+} + {}^{\bullet}OOH + H^+, \quad k_2 = 0.002\ L\ mol^{-1}\ s^{-1} \tag{2}$$

Step 2 has a low-rate constant and is thus a rate-limited reaction process. The increase of k_2 will probably bring a remarkable improvement in catalytic cycle efficiency. To realize this, a new kind of active metal center is essential. It should also possess variable valence states, and high valence ions must be reduced more quickly. This idea leads to the selection of Co_3O_4 NPs as mimic peroxidases.

Because Co has similar properties to Fe, Co compounds have been used in H_2O_2 catalytic reactions in place of Fe compounds

Received: November 8, 2013
Accepted: January 3, 2014
Published: January 3, 2014

dx.doi.org/10.1021/am405009f | ACS Appl. Mater. Interfaces 2014, 6, 1959−1970

for a long time and have shown excellent catalytic activity.[11−16] These studies mainly concentrated on Co ions (principally Co^{2+}) or Co ions chelated by EDTA (ethylene diaminetetraaceticacid), DTPA (diethylenetriaminepentaacetic acid), NTA (nitrilotriacetate), or other chelators. Mechanisms were also analyzed in these studies, but different conclusions were obtained with different binding state of Co^{2+}. Co^{2+}, with or without the presence of chelators, differed widely in its ability to catalyze radicals generated from H_2O_2.[11−13] Cobalt oxide NPs with different morphologies (such as cubes,[17] sheets,[18] wires,[19] tubes,[20] and so forth[21−24]) are used in Li ion batteries, gas sensors, and catalysts for CO oxidation and hydrocarbon compound combustion. Recently, Co_3O_4 NPs prepared using the solvothermal method expressed catalytic activities to H_2O_2 similar to those of Fe_3O_4 NPs.[25] Co_3O_4 NPs have already showed their potential as enzyme mimetics in H_2O_2 reactions, but the mechanism hasn't been completely clarified.

In this work, Co_3O_4 NPs were prepared by the coprecipitation method and modified by dimercaptosuccinic acid (DMSA) to be highly soluble in water. The enzyme-like activity of prepared Co_3O_4 NPs was detected in various conditions and compared with analogous Fe_3O_4 NPs. Multienzyme catalytic properties, including catalase, peroxidase, and SOD-like activities, were characterized in detail. The electron spin resonance (ESR) method was used to provide direct evidence of the catalytic activities of Co_3O_4 NPs and to support mechanism analysis. On the basis of their high peroxidase-like activity, an immunohistochemical assay was designed to verify the promising applicability of Co_3O_4 NPs.

2. EXPERIMENTAL SECTION

Materials. $Co(NO_3)_2{\cdot}6H_2O$ was purchased from Shantou Xilong Chemical Ltd. Aqueous ammonia, dimercapto succinic acid (DMSA), sodium phosphate dibasic, sodium chloride, sodium borate, and boric acid were provided by Shanghai Lingfeng Chemical Reagent Co. Ltd. Hydrogen peroxide (H_2O_2, 30%) was received from Shanghai Aladdin Chemical Ltd. 3,3′,5,5′-Tetramethylbenzidine (TMB), 1-(3-dimethylamino-propyl)-3-ethyl carbodiimide hydrochloride (EDC), and *N*-hydroxysuccinimide were purchased from Sigma-Aldrich. Avastin antibody was purchased from Roche. Diaminobenzidine (DAB), pepsin, and hematoxylin were produced by Fuzhou MaiXin biotechnology development Co. Ltd. VEGF IHC kit was purchased from Beyotime biotechnology Co. Ltd. Deionized water was used throughout the study.

Synthesis of Co_3O_4 NPs. Preparation of Co_3O_4 NPs was according to Zhang's work[26] with some modification. $Co(NO_3)_2{\cdot}6H_2O$ (0.291 g) and aqueous ammonia (0.81 mL, 25%) was mixed in 50 mL of water in a 100 mL three-neck flask. H_2O_2 (60 μL, 30%) was added under stirring to obtain $[Co(NH_3)_6]^{3+}$ solution. Another 15 min of stirring in a 60 °C water bath was performed to ensure that Co^{2+} was thoroughly oxidized to Co^{3+} and excess hydrogen peroxide was decomposed. $Co(NO_3)_2{\cdot}6H_2O$ (0.145 g), dissolved in 20 mL of water, was poured into the solution. The mixture reacted for 3 h under stirring (1000 rpm) at 60 °C and then cooled down to room temperature. Black precipitates were collected by centrifugation and washed with water three times before being dissolved in 50 mL of water for the next use.

Synthesis of DMSA-Modified Co_3O_4 NPs. Co_3O_4 precipitates (dissolved in 50 mL of water) were sonicated for 10 min, and then the pH was adjusted to 2.0−3.0 by HCl (0.1 M). DMSA (0.045 g) was dissolved in 1 mL of DMSO and mixed with the Co_3O_4 suspension under stirring (1000 rpm). The mixture was sonicated for 2 h and stirred for 5 h. Precipitates were collected again via centrifugation and washed three times before being dissolved in 50 mL of water. The pH was adjusted to 9.0−10.0 by NaOH (0.1 M), and then the mixture was sonicated for 5 min and turned into a stable and clear solution. After that, the pH of the solution was adjusted to 7.0 by HCl (0.1 M), and the solution was dialyzed for 3 days to remove excess DMSA and other impurities. The final sample (Co_3O_4) was filtered through a 0.22 μm membrane and stored at 4 °C.

Fe_3O_4 NPs that possess similar properties were also synthesized by the coprecipitation method according to our previous work.[27]

Catalase-like Activity Assay. The catalase-like activity of Co_3O_4 NPs in different pH solutions (pH 3.6, pH 7.4, and pH 11.0) was evaluated in 10 mL buffers (0.02 M) with 0.99 μg/mL Co_3O_4 NPs and 1 M H_2O_2. Dissolved oxygen was monitored after the addition of H_2O_2 by a multi-parameter water quality meter (DZS-708, SHJK). To eliminate the intrinsic differences between H_2O_2 decomposition in different pH solutions, the same process was conducted without the addition of Co_3O_4 NPs in corresponding buffers. The results were the differences between the two experiments in the same pH.

The comparison of catalase-like activity between Co_3O_4 and Fe_3O_4 NPs was carried out in 10 mL of buffer (0.02 M, pH 7.4) with 1 M H_2O_2 and the same concentration (0.99 μg/mL) of Co_3O_4 or Fe_3O_4 NPs. Dissolved oxygen was monitored after the addition of NPs by a multi-parameter water quality meter (DZS-708, SHJK). The same reaction system without NPs was tested as a control.

Steady-State Kinetic Analysis of Co_3O_4 NPs as Peroxidase. The steady-state kinetic assays were carried out at room temperature in 250 μL of reaction buffer (0.2 M, pH 3.6) with 0.33 μg (in terms of Co weight) of Co_3O_4 in the presence of H_2O_2 and TMB. The kinetic analysis of Co_3O_4 with TMB as the substrate was performed by varying the concentrations of TMB at a fixed H_2O_2 concentration and vice versa.

All the reactions were monitored in time scan mode at a 650 nm wavelength every 30 s during the first 3 min by the BIO-RAD680 Microplate Reader. The reaction rates were then obtained by calculating the slopes of initial absorbance chances with time. All measurements were performed at least in triplicate, and the values were averaged. Results were given as means ± the standard deviation (SD). Catalytic parameters were determined by fitting data to the Michaelis-Menten equation.

$$v = \frac{v_{max}[S]}{K_m + [S]} \tag{3}$$

In this equation, v is the rate of conversion, v_{max} is the maximum rate of conversion, $[S]$ is the substrate concentration, and K_m is the Michaelis constant, which is equivalent to the substrate concentration in which the rate of conversion is half of v_{max}. Fe_3O_4 NPs were tested in an analogous process for comparison purposes.

The direct comparison of peroxidase-like activity between Co_3O_4 and Fe_3O_4 NPs was carried out in 250 μL of reaction buffer (0.2 M, pH 3.6) with 0.4 mg/mL TMB, 1.28 M H_2O_2, and Co_3O_4 or Fe_3O_4 NPs of the same concentration (1.32 μg/mL). The absorbance was monitored with time.

ESR Spectroscopy Measurements. ESR measurements were performed using a Bruker EMX ESR spectrometer (Billerica, MA) at room temperature under the following conditions: 1 G field modulation, 100 G scan range, and 20 mW microwave power for detection of spin adducts using spin trap BMPO and 0.04 G field modulation, 5 G scan range, and 1 mW microwave power for ESR oximetry using the spin label ^{15}N-PDT. Fifty microliter aliquots of control or sample solutions were put in glass capillary tubes with internal diameters of 1 mm and sealed. The capillary tubes were inserted into the ESR cavity, and the spectra were recorded at selected times. Since the ESR method is very sensitive and may be affected by DMSA, naked Co_3O_4 NPs were used in this part rather than the DMSA-coated Co_3O_4 NPs used in other parts of the work.

ESR spin label oximetry is a quantitative approach to measure oxygen content using the water-soluble spin label ^{15}N-PDT. The hydrogen peroxide solution was mixed with ^{15}N-PDT in buffers of different pH (pH 3.6, pH 7.4, pH 11.0) containing catalase or Co_3O_4 NPs. To verify the ability of Co_3O_4 NPs to scavenge superoxide anions, xanthine and xanthine oxidase (XOD) were mixed in PBS buffer (pH 7.4) to generate a superoxide and BMPO was used to trap

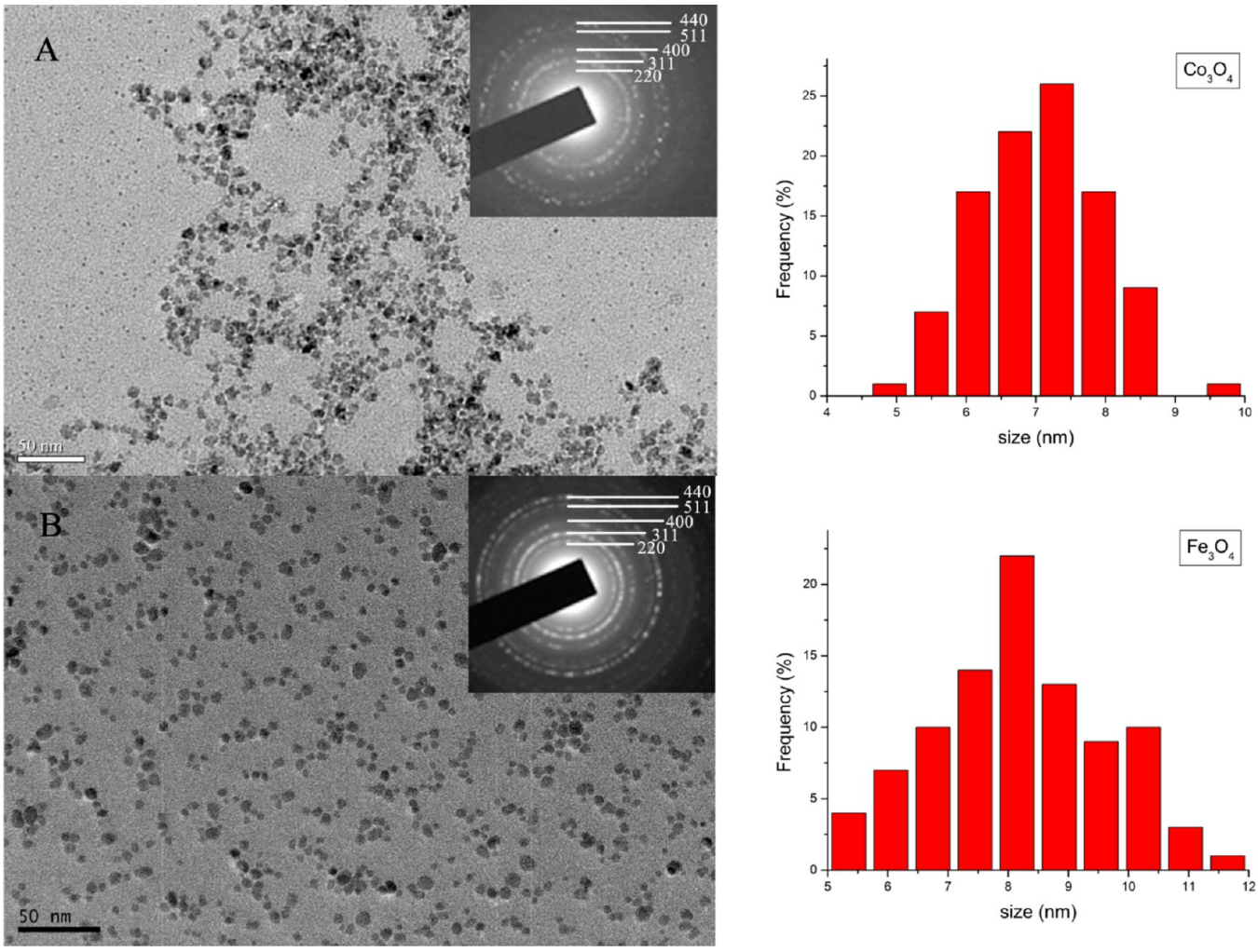

Figure 1. TEM images, electron diffraction patterns, and size distributions of (A) Co_3O_4 and (B) Fe_3O_4 NPs.

the superoxide in the form of spin adduct BMPO/•OOH. The reaction was started by adding XOD. For hydroxyl radical (•OH) detection under various conditions, BMPO was employed to trap •OH to form the BMPO/•OH spin adduct.[28] The hydrogen peroxide solution was mixed with BMPO in acidic buffer (pH 3.6) and was detected after the addition of Co_3O_4 NPs or control solutions.

Bioconjugation of Co_3O_4 NPs with Avastin Antibody. The bioconjugation of Co_3O_4 NPs with the avastin antibody was realized through the EDC/NHS strategy, as previously reported.[27] EDC (100 μL, 10 mg/mL), NHS (70 μL, 10 mg/mL), and DMSA-coated Co_3O_4 NPs (1 mL, 0.33 mg/mL) were mixed in 0.5 mL of borate buffer (0.02 M, pH 9.0). The mixture was shaken at 25 °C for 30 min. The coupling reaction was started by adding 20 μL of avastin antibody (25 mg/mL), and then the mixture was continually shaken for a further 2 h at 25 °C. The Ab-Co_3O_4 conjugates were purified by gel chromatography (GE sephacryl s-300) to remove excess antibody and were stored at 4 °C. BSA-Co_3O_4 conjugates were prepared in the same process to act as a contrast in immunohistochemistry.

The component analysis of the Ab-Co_3O_4 conjugates included two steps. The quantitative analysis of Co was conducted using the 5-Cl-PADAB method,[29] and then Ab-Co_3O_4 conjugates and Co_3O_4 NPs were both diluted to a certain concentration (15 μg/mL). A BCA assay[30] was then performed to calculate the amount of antibody by comparing the two samples.

Immunohistochemistry Experiments Based on the Peroxidase Activity of Ab-Co_3O_4 Conjugates. The immunohistochemistry experiments were designed to detect vascular endothelial growth factor (VEGF) overexpressed in the cytoplasm of esophageal cancer cells. Since Co_3O_4 was conjugated with avastin antibody, DAB was used as the chromogenic substrate. An experimental group (Ab-Co_3O_4) and three control groups (Ab-Co_3O_4 after free avastin antibody blocking, BSA-Co_3O_4, and PBS) were set up to prove the practicality of Co_3O_4 NPs in bioassay.

Paraffin sections of tumor tissues were submerged in dimethylbenzene three times, each for 10 min, and then in 100% ethanol twice, each for 10 min. Different levels of alcohol (90−70%) were followed, also each for 10 min, and then the tumor sections were placed in distilled water for 10 min. After that, they were taken out and water around the tissues was wiped off. H_2O_2 (3%) was added to the tissues, and they were placed in darkness for 15 min to seal off the endogenic peroxidase. The sections were washed with water and submerged in PBS buffer (pH 7.4) three times, each for 5 min. A total of 50 μL of pepsin was added, and the tissues were kept at 37 °C for 30 min. They were washed again twice with PBS and were divided into five groups.

The experimental group was incubated with Ab-Co_3O_4 (100 μL, 15 μg/mL). One of the control groups was stained with a commercial VEGF IHC kit, in which natural HRP was used as the enzyme label. One of the control groups was incubated with avastin (100 μL, 5 mg/mL) to block antigen sites and then with Ab-Co_3O_4 (100 μL, 15 μg/mL). The other two control groups were incubated with BSA-Co_3O_4 (100 μL, 15 μg/mL) or PBS (100 μL), respectively. They were all kept at 37 °C for 30 min. Afterwards, all of them were washed with excessive PBS to remove unbonded NPs and treated with DAB and H_2O_2 mixture (100 μL, dissolved in acidic buffer) for 15 min.

After being washed with PBS twice, they were counterstained with hematoxylin, and then the sections were dehydrated using alcohol (70−100%), each for 10 min. After vitrification by dimethylbenzene

dx.doi.org/10.1021/am405009f | ACS Appl. Mater. Interfaces 2014, 6, 1959−1970

Table 1. Hydrodynamic Size and Zeta-Potential Data (measured in different pH's)[a]

	size by DLS (nm)			zeta potential (mV)		
	pH 3.6	pH 7.4	pH 9.0	pH 3.6	pH 7.4	pH 9.0
Fe_3O_4	69.3 ± 1.0	62.5 ± 0.6	53.2 ± 0.4	−29.98 ± 5.12	−39.31 ± 10.77	−43.28 ± 3.98
Co_3O_4	58.1 ± 1.4	53.5 ± 0.8	48.6 ± 0.3	−26.15 ± 5.25	−34.25 ± 5.19	−39.74 ± 4.32
Ab-Co_3O_4	–	87.6 ± 1.3	–	–	−14.16 ± 3.14	–

[a]Ab-Co_3O_4 refers to Co_3O_4 NPs and avastin antibody conjugates.

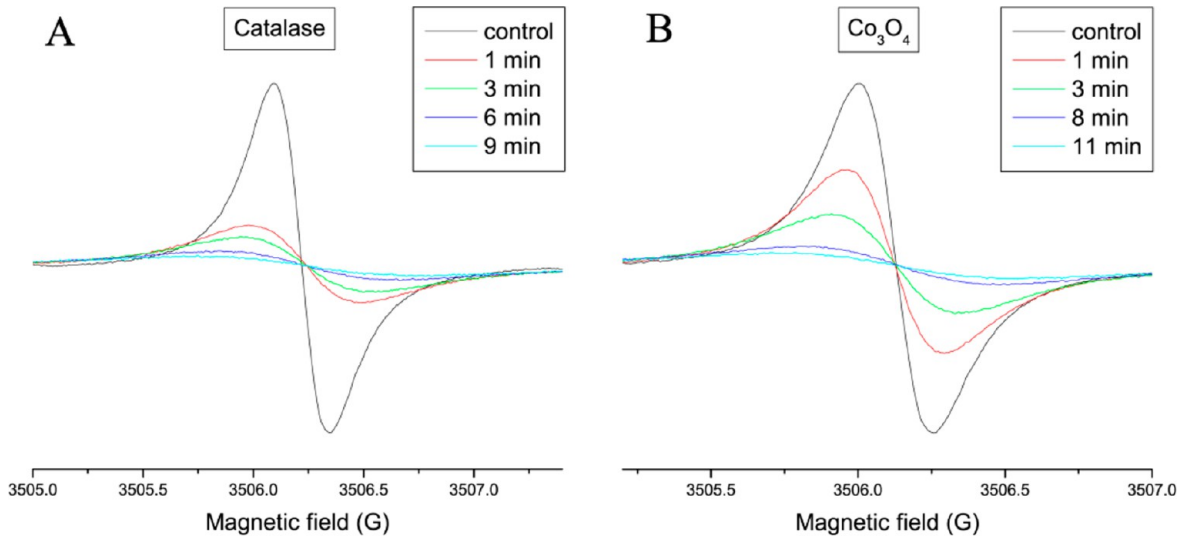

Figure 2. Catalase-like activity of Co_3O_4 NPs. Oxygen generation is measured in a closed chamber with samples of 0.1 mM ^{15}N-PDT, 10 mM H_2O_2, and (A) 10 unit/mL catalase or (B) 1.7 μg/mL Co_3O_4 NPs mixed with different time intervals compared with (black) catalyst blank controls in 10 mM pH 7.4 PBS.

three times, the sections were sealed with balsam and observed under a microscope (AXIOVERT200, ZEISS).

Characterization. The size and morphology of Co_3O_4 and Fe_3O_4 NPs were determined by transmission electronic microscopy (TEM, JEOL JEM-2100). Samples were dropped onto a carbon-coated copper grid and dried at room temperature. Electronic diffraction was used to determine the crystalline structure of the NPs. The hydrodynamic size and zeta-potential was measured by dynamic light scattering (DLS Zeta-Size 3000HS).

3. RESULTS AND DISCUSSION

3.1. Characterization of Prepared Co_3O_4 NPs and Fe_3O_4 NPs. TEM images of as-prepared DMSA-coated Co_3O_4 NPs and DMSA-coated Fe_3O_4 NPs are showed in Figure 1. The average size of Co_3O_4 NPs is approximately 7.2 nm while Fe_3O_4 NPs, which were also synthetized by the co-precipitation method, are 8.1 nm. The diffraction rings that appeared in electronic diffraction patterns could be indexed to theory values of their typical lattice planes, such as {220}, {311}, {400}, {511}, and {440} from the inverse cubic spinel structure of Fe_3O_4 or Co_3O_4. This suggested that both samples possessed the same crystal structure.[31] The hydrodynamic size and zeta-potential data are shown in Table 1. Both of the samples display much larger hydrodynamic sizes than their magnetic core sizes obtained from TEM observation, suggesting that Fe_3O_4 and Co_3O_4 NPs may exist in clusters in aqueous solutions. Due to the electrostatic repulsion caused by high negative surface charges, the samples have good dispersion in aqueous solutions. Stability testing was conducted for at least 3 months, and no precipitation or turbid phenomena were observed.

3.2. Catalase-like and SOD-like activities of Co_3O_4 NPs. To investigate the catalytic activity of Co_3O_4 NPs, we choose 3,3′,5,5′-tetramethylbenzidine (TMB) as the chromogenic substrate, which is often used to demonstrate the peroxidase-like activity of other NPs. Experiments were performed by catalyzing the oxidation of TMB in the absence of H_2O_2. Since pH has been reported to have a significant effect on the activity of mimic enzyme NPs, the activity of Co_3O_4 NPs was first measured in buffers of different pH (from 3 to 11). As shown in Figure S1, TMB could be oxidized in acidic conditions, and this revealed that Co_3O_4 NPs possess peroxidase-like activity. When neutral or alkaline buffers were used, there was no color transformation but bubbles appeared. This might have resulted from H_2O_2 decomposition catalyzed by Co_3O_4 NPs.

ESR oximetry was conducted to further confirm the oxygen production in hydrogen peroxide decomposition catalyzed by catalase and Co_3O_4 NPs. The ESR oximetry measurement is based on the bimolecular collision of oxygen and a spin probe. Since oxygen is paramagnetic, the collision between oxygen and a spin probe (^{15}N-PDT) results in shorter relaxation times. Consequently, ESR signals with broader line widths are observed for the spin probe. The integrated area of the ESR signal over the scanning range is unaffected by this effect on the relaxation time, so the broadening of the spin probe's ESR signal is accompanied by a decrease in the peak height of the ESR signal. When the ESR signal is measured with a small amount of oxygen, a narrower line width and higher peak intensity is observed compared to the measurement of the ESR signal under more oxygenated conditions. As shown in Figure 2, a concentration-dependent increase in line width and decrease in the peak intensity of the ESR signal indicates oxygen formation when catalase or Co_3O_4 NPs catalyze H_2O_2

decomposition. This supports the theory that Co_3O_4 NPs possess catalase-like activity. This kind of activity has also been reported in some other nanomaterials, such as Au@Pt NPs,[32] RuO_2 NPs,[33] and ferritin−platinum NPs.[34]

Further ESR study showed that Co_3O_4 NPs could exhibit catalase-like activity not only in neutral conditions but also in acidic and alkaline conditions (Supporting Information Figure S2). Dissolved oxygen generation was also detected in buffers of different pH values (3.6, 7.4, 11.0) with an oxygen electrode, showing that the catalase-like activity of Co_3O_4 NPs increased as the pH value increased (Figure 3).

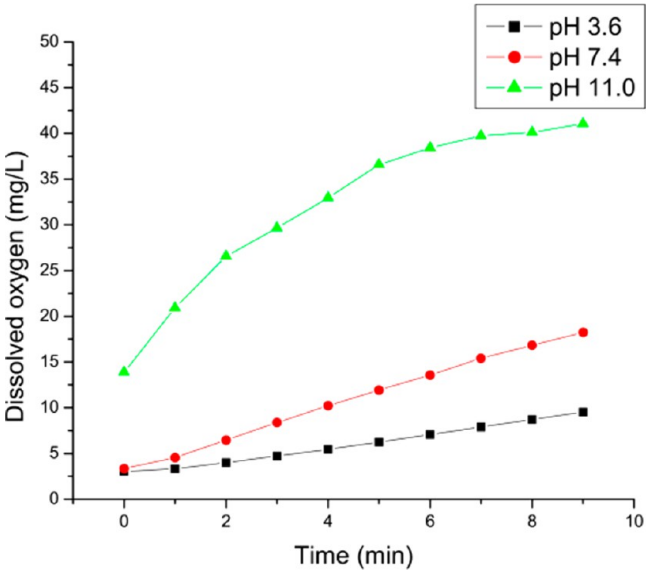

Figure 3. Dissolved oxygen generation catalyzed by Co_3O_4 NPs in different pHs. Data were the difference between the results from samples containing 1 M H_2O_2, 0.2 M buffer with or without 0.99 μg/mL Co_3O_4 NPs.

As we all know, H_2O_2 is an active molecule and tends to decompose slowly. The addition of Co_3O_4 NPs can accelerate the decomposition, especially in neutral and alkaline conditions. Since the redox potential of H_2O_2/O_2 is very low in a high pH, H_2O_2 is more easily oxidized by Co^{3+}. The reaction can be described by the following equations:

$$2Co^{3+} + H_2O_2 + 2OH^- \rightarrow 2Co^{2+} + 2H_2O + O_2\uparrow \quad (4)$$

$$2Co^{2+} + H_2O_2 \rightarrow 2Co^{3+} + 2OH^- \quad (5)$$

The comparison of catalase-like activity between Co_3O_4 and Fe_3O_4 NPs is shown in Figure 4. In the absence of Co_3O_4 NPs, the dissolved oxygen value showed a very weak increase, due to the slow decomposition of H_2O_2 itself. The dissolved oxygen rate increased rapidly in the presence of Co_3O_4 NPs, while Fe_3O_4 NPs showed very weak activity in the same experimental conditions. This was probably because the redox potential of Co^{3+}/Co^{2+} (standard redox potential 1.808 V) is much higher than that of Fe^{3+}/Fe^{2+} (standard redox potential 0.771 V), and Co^{3+} possesses a higher oxidation capacity.[35,36] As a result, the rate of Reaction 3 is higher than that of Reaction 5. Co_3O_4 NPs showed much higher catalase-like activity than analogous Fe_3O_4 NPs with the same size, surface modification, zeta potential, and crystal structure.

$$2Fe^{3+} + H_2O_2 + 2OH^- \rightarrow 2Fe^{2+} + 2H_2O + O_2\uparrow \quad (6)$$

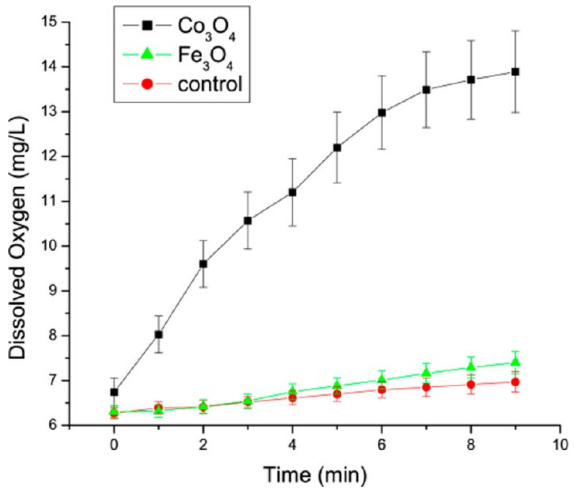

Figure 4. Comparison of catalase-like activity between Co_3O_4 and Fe_3O_4 NPs. The curves show dissolved oxygen generation with time in different catalytic reaction systems. The samples contained 1 M H_2O_2 and 0.2 M buffer (pH 7.4) with the same concentration (0.99 μg/mL) of Co_3O_4 and Fe_3O_4 NPs. Pure water was used instead of NPs as a control. The error bars represent the standard deviation of three measurements.

$$2Fe^{2+} + H_2O_2 \rightarrow 2Fe^{3+} + 2OH^- \quad (7)$$

Besides decomposing H_2O_2, Co_3O_4 NPs also exhibited superoxide scavenging activity. Superoxides were generated in situ by the xanthine/xanthine oxidase system (Xan/XOD).[37] BMPO was chosen as a spin trap to form the spin adduct with superoxide-designated BMPO/$^{\bullet}$OOH. The ESR spectrum characteristic for this spin adduct has four lines with relative intensities of 1:1:1:1 and hyperfine splitting parameters of aN $^1/_4$ 13.4 and abH $^1/_4$ 12.1 (shown in Figure 5).[38] The addition of SOD resulted in a significantly decreased ESR signal intensity due to SOD's strong ability to dismutate superoxides.

A similar phenomenon was observed when Co_3O_4 NPs were added. The ESR signal decreased along with the increasing

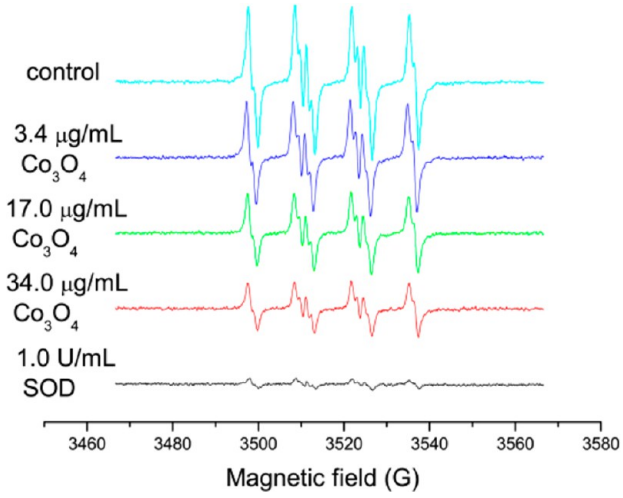

Figure 5. SOD-like activity of Co_3O_4 NPs. ESR spectra were recorded from samples containing 10 mM PBS, 1 mM Xanthine, 0.05 mM DTPA, and 0.2 U/mL XOD, without (control) and with 3.4 μg/mL, 17 μg/mL, and 34 μg/mL Co_3O_4 NPs and 1.0 U/mL SOD. All the spectra were obtained 2 min after mixing.

Table 2. Kinetic Parameters of Fe_3O_4 and Co_3O_4 NPs[a]

	[E] (M)	substrate	K_m (mM)	V_{max} (10^{-7} × M s^{-1})	k_{cat} (s^{-1})	k_{cat} (S s^{-1} nm^{-2})
Fe_3O_4	7.92×10^{-9}	TMB	0.233 ± 0.006	1.76 ± 0.01	22.22 ± 0.13	0.108 ± 0.006
Fe_3O_4	7.92×10^{-9}	H_2O_2	479.91 ± 117.36	2.75 ± 0.36	34.72 ± 4.55	0.168 ± 0.022
Co_3O_4	2.53×10^{-9}	TMB	0.103 ± 0.015	2.56 ± 0.08	101.19 ± 3.16	0.622 ± 0.019
Co_3O_4	2.53×10^{-9}	H_2O_2	173.51 ± 57.23	1.89 ± 0.22	74.70 ± 8.70	0.459 ± 0.053

[a][E] is the particle concentration, K_m is the Michaelis constant, V_{max} is the maximal reaction velocity, and k_{cat} is the catalytic constant, where $k_{cat} = V_{max}/[E]$.

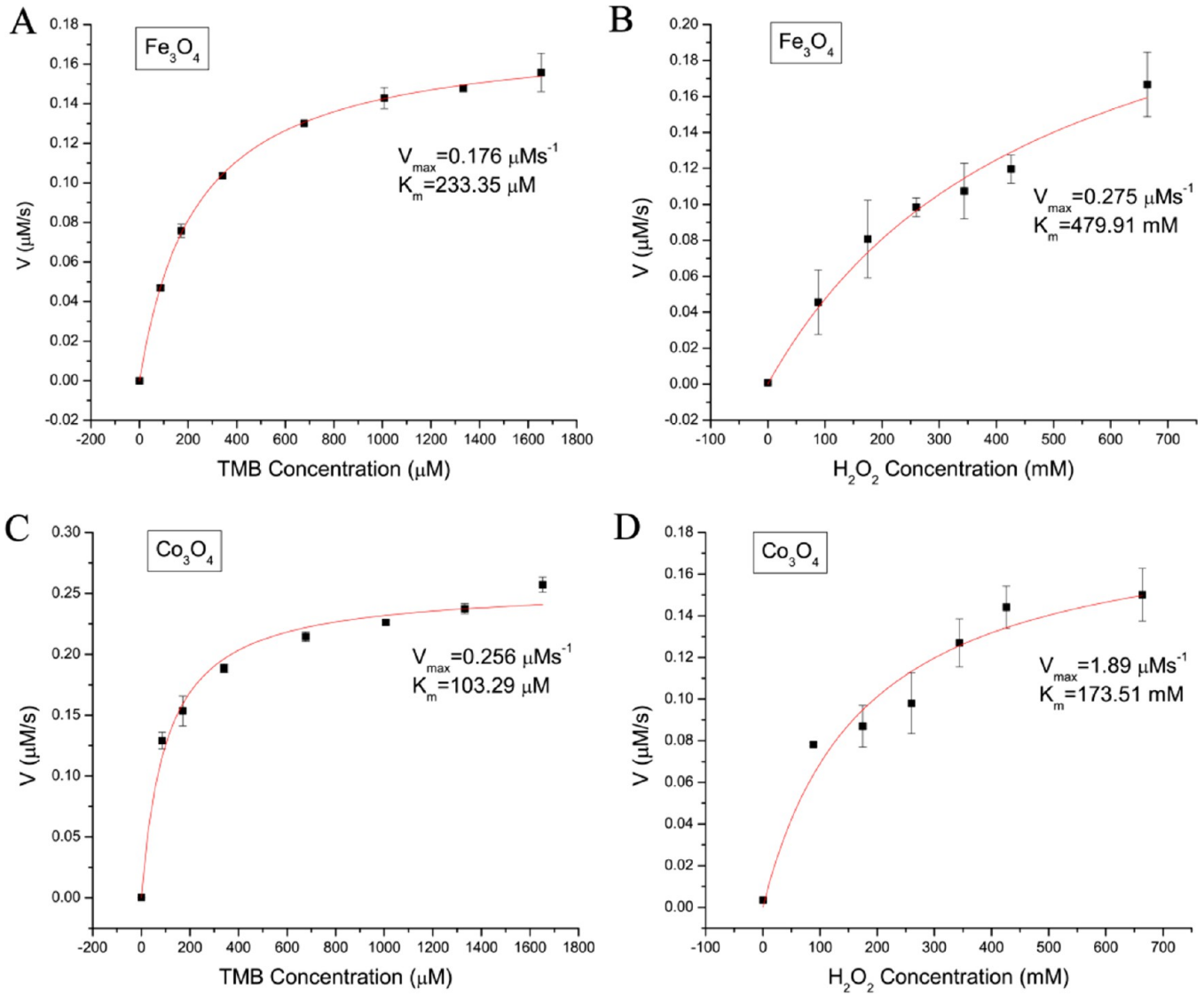

Figure 6. Kinetic analysis of Fe_3O_4 NPs with TMB (A) or H_2O_2 (B) and Co_3O_4 NPs with TMB (C) or H_2O_2 (D). For A and C, the H_2O_2 concentration was 663.8 mM while the TMB concentration varied. For B and D, the TMB concentration was 1653.4 μM while the H_2O_2 concentration varied. Absorbance data were back calculated to concentration by the Beer–Lambert Law using a molar absorption coefficient of 39 000 M^{-1} cm^{-1} for TMB-derived oxidation products.[39] Reaction rates at different concentrations of substrate were obtained by calculating the slopes of initial absorbance changes with time. Error bars represent the standard deviation of three repeated measurements.

concentration of Co_3O_4 NPs, suggesting that Co_3O_4 NPs possess SOD-like activity. The mechanism hasn't been verified because intermediates of the reaction, except for O_2, are difficult to identify. Possible mechanisms for these phenomena are proposed in eqs 7 and 8. We infer that the reaction may also be accompanied by the H_2O_2 decomposition reaction, leading to superoxides finally decomposed into O_2 and H_2O.

In summary, Co_3O_4 NPs can act as efficient scavengers for both H_2O_2 and superoxides in neutral and alkaline conditions.

$$Co^{3+} + {}^{\bullet}OOH \rightarrow Co^{2+} + O_2\uparrow + H^+ \quad (8)$$

$$Co^{2+} + {}^{\bullet}OOH + H^+ \rightarrow Co^{3+} + H_2O_2 \quad (9)$$

3.3. Peroxidase-like Activity of Co_3O_4 NPs. Peroxidase-like activity in an acidic buffer (pH 3.6) was evaluated by performing steady-state kinetic analysis. Catalytic parameters (Table 2) were obtained by fitting the data into the Michaelis–

Menten equation (curves shown in Figure 6, double-reciprocal plots shown in Supporting Information Figure S3).

The K_m value of Co_3O_4 NPs for TMB was half lower than that of Fe_3O_4 NPs, suggesting that Co_3O_4 NPs have an apparently higher affinity to TMB. The K_m values of Co_3O_4 NPs for H_2O_2 were also much lower than those for Fe_3O_4 NPs, which means a lower concentration of H_2O_2 was required to obtain maximal reaction velocity for Co_3O_4 NPs. The advantages of Co_3O_4 NPs in catalytic efficiency were also identified since their k_{cat} values for TMB and H_2O_2 were significantly higher than those of Fe_3O_4 NPs. Here k_{cat} is the catalytic constant calculated in terms of nanoparticle units.

Since the peroxidase-like activity of NPs originates mainly from metal ions on the surface of the particles, NP size has a significant impact on the k_{cat}. Larger particles have larger surfaces and can expose more catalytically active sites. Yan et al.'s Fe_3O_4 NPs were about 300 nm while our Co_3O_4 NPs were only 7.2 nm in size, which explains why the k_{cat} value (with TMB as the substrate) of Yan et al.'s[4] Fe_3O_4 NPs is higher than that of our Co_3O_4 NPs. In order to eliminate the impact of differences in particle size, the k_{cat} value was normalized using particle surface area S. As shown in Table 2, the obtained k_{cat}/S value of Co_3O_4 for TMB was much higher than that of Yan et al.'s Fe_3O_4 NPs (0.11 s^{-1} nm^{-2}), and the k_{cat}/S values of Co_3O_4 for TMB and H_2O_2 were several times larger than that of our Fe_3O_4 NPs.

A direct peroxidase-like activity comparison experiment between Co_3O_4 and Fe_3O_4 NPs is also shown in Figure 7, indicating clearly that a great improvement in peroxidase-like activity was achieved by employing Co_3O_4 NPs as catalysts.

The mechanism of Co_3O_4 NPs as peroxidase mimetics was verified using the ESR method. The results (Figure 8) showed that, unlike Fe_3O_4 NPs in our previous work,[40] Co_3O_4 NPs didn't enhance $^{\bullet}OH$ generation in acidic condition. Co_3O_4 NPs coated by DMSA even showed $^{\bullet}OH$ scavenging activity (Supporting Information Figure S4), probably due to the reducibility of DMSA molecules. So Co_3O_4 NPs don't react with H_2O_2 by Fenton reaction.

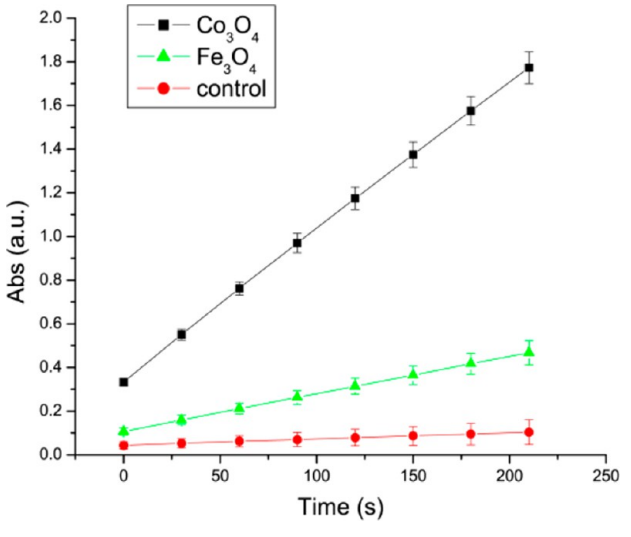

Figure 7. Comparison of peroxidase-like activity between Fe_3O_4 and Co_3O_4 NPs. The curves show absorbance variation with time at 650 nm wavelength in different catalytic reaction systems. The samples contained 1.27 M H_2O_2, 0.4 mg/mL TMB, and 0.2 M buffer (pH 3.6) with the same concentration (1.31 μg/mL) of Co_3O_4 and Fe_3O_4 NPs. Pure water was tested as a control. The error bars represent the standard deviation of three measurements.

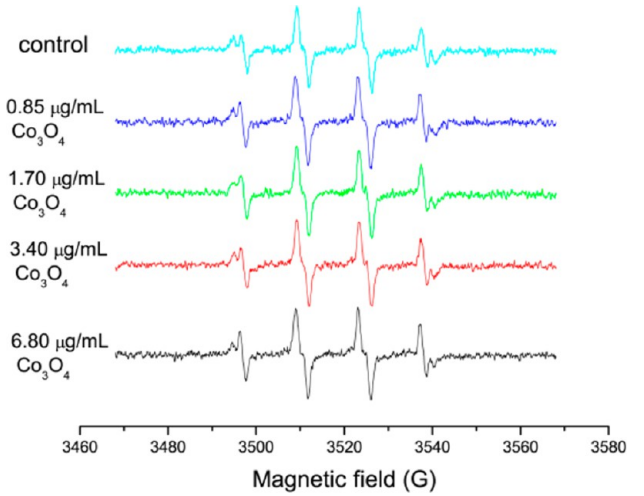

Figure 8. Effect of Co_3O_4 NPs on hydroxyl radical generation. ESR spectra were obtained from samples containing 25 mM BMPO, 10 mM H_2O_2, and 10 mM buffer (pH 3.6) with naked Co_3O_4 NPs of different concentrations. All the spectra were recorded 5 min after mixing.

Previous reports[11,12] also demonstrated that Co^{2+} doesn't efficiently produce $^{\bullet}OH$ from H_2O_2, due to the high redox potential of Co^{3+}/Co^{2+}.[41] Since Co_3O_4 is a kind of semiconductor material, we suspected that Co_3O_4 NPs may have worked as electron transfer mediators. Cytochrome c (cyt c) was used to test the accepting electron capability of Co_3O_4 NPs because cyt c is an active reactant in the electron transfer process. The original spectrum of cyt c (in pH 3.6 buffer) is shown in Figure 9 (black line), with two absorption peaks at 520 nm and 550 nm that suggest that cyt c is in a reduced state. Co_3O_4 NPs were added and reacted for 1 h before they were

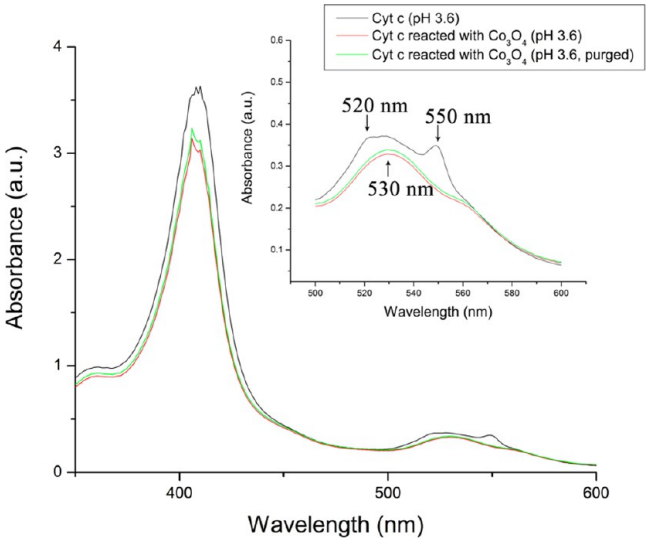

Figure 9. UV−visible spectrum of original cyt c (black line), cyt c reacted with Co_3O_4 NPs (red line), and cyt c reacted with Co_3O_4 NPs under deoxygenated condition. The inset shows a scale expanded from 450 to 600 nm. The samples contained 0.2 M buffer (pH 3.6) and 6 mg/mL cyt c. A total of 3.4 μg of Co_3O_4 NPs were added to react with cyt c and were removed thoroughly by centrifugation.

dx.doi.org/10.1021/am405009f | ACS Appl. Mater. Interfaces 2014, 6, 1959−1970

removed by centrifugation. The spectrum of cyt c is shown in Figure 9 (red line). The original two peaks disappeared with the evolution of a new peak at 530 nm, revealing that cyt c was oxidized. In order to know whether cyt c was oxidized by dissolved oxygen, we purged Co_3O_4 NPs solution, acidic buffer (0.2 M, pH 3.6), and the water used to dissolve cyt c with pure nitrogen for 0.5 h and then repeated the same process. Still cyt c was oxidized (Figure 9, green line), which proved that Co_3O_4 NPs were able to obtain electrons from cyt c and the reaction doesn't rely on dissolved oxygen.

So we proposed an electron transfer mechanism. The main difference between our mechanism and the Fenton reaction is that the substrate is oxidized directly by Co^{3+}, not by radicals generated from H_2O_2. As shown in Scheme 1, Co^{3+} first gets an

Scheme 1. Possible Mechanism of Co_3O_4 NPs as Peroxidase

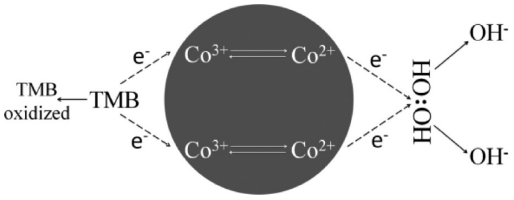

electron from TMB and turns into Co^{2+}, making TMB oxidize into a blue derivative. Co^{2+} passes the electron to H_2O_2 and turns back to Co^{3+}. H_2O_2 gets two electrons and decomposes into OH^-. The whole process can be written as the following equations:

$$2Co^{3+} + TMB \rightarrow 2Co^{2+} + TMB(oxidized) + 2H^+ \quad (10)$$

$$Co^{2+} + H_2O_2 + 2H^+ \rightarrow Co^{3+} + 2H_2O \quad (11)$$

The redox potential of H_2O_2 in our reaction system can be calculated using the Nernst equation.

$$\varphi_{H_2O_2} = \varphi_{H_2O_2} + RT/nF \ln(c_{H_2O_2} \times c_{H^+}) = 1.776 + \frac{0.0592}{2} \ln(1.27 \times 10^{-3.6\times2}) = 1.566 \quad (12)$$

TMB is an excellent redox indicator that possesses a well-established value of 1.13 ± 0.01 V.[42,43] The standard redox potential of Co^{3+}/Co^{2+} is 1.808 V, but the coordination of oxygen in the Co_3O_4 crystal is widely assumed to reduce that value.[11−13] Though the redox potential of Co^{3+}/Co^{2+} in our Co_3O_4 NPs hasn't been measured, the value in similar samples is reported to be around 1.30 V.[44,45] The order of H_2O_2, Co_3O_4, and TMB redox potentials make the process mentioned above happen smoothly (showed in Scheme 2). As for Fe_3O_4, the redox potential of Fe^{3+}/Fe^{2+} is, at most, 0.771 V. The electron can be passed from Fe_3O_4 NPs to H_2O_2, but it can't be passed from TMB to Fe_3O_4 NPs, so the TMB oxidation is mainly dependent on $^{\bullet}OH$ from H_2O_2 when Fe_3O_4 NPs are used as catalysts.

In order to verify this mechanism, the oxidizability of Co_3O_4 NPs was detected by mixing Co_3O_4 NPs only with TMB in different buffers. Without H_2O_2, TMB almost couldn't be oxidized in water (control groups). Neither could it be oxidized by Fe_3O_4 NPs, since the Fenton reaction depends mainly on radicals generated from H_2O_2. As to Co_3O_4 NPs, a color reaction didn't happen in alkaline and neutral buffers, but in an acidic buffer we can see that TMB is oxidized, although it reacts

Scheme 2. Theoretical Analysis of the NPs as Peroxidase

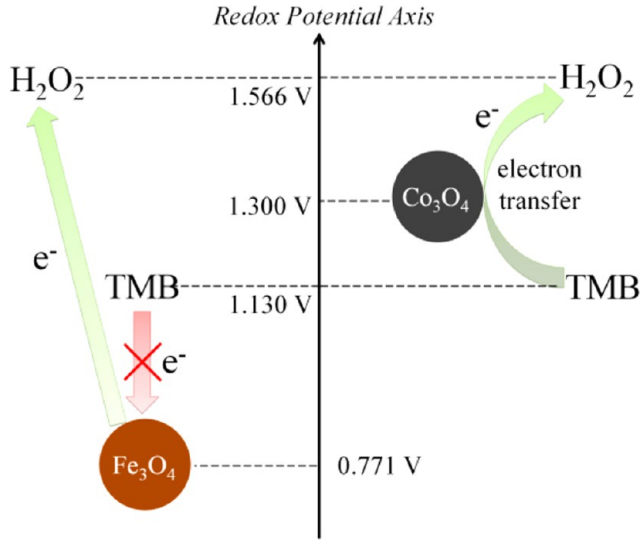

very slowly (Figure 10). Under the deoxygenated condition, the same color reaction was observed, confirming again that Co_3O_4

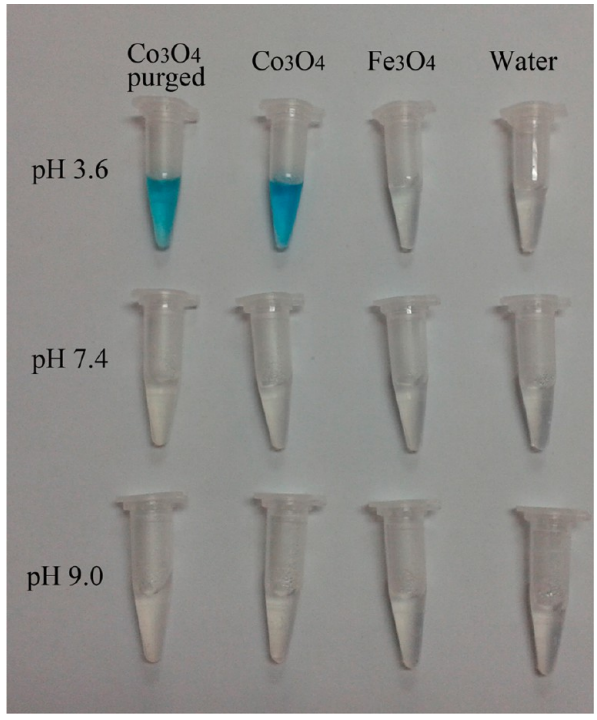

Figure 10. Co_3O_4 NPs can oxidize TMB without H_2O_2 in acidic conditions. All the samples contained 0.2 M buffer (pH 3.6) and 0.2 mg/mL TMB with or without 6 μg/mL NPs. In the first column, Co_3O_4 NPs and acidic buffer (0.2 M, pH 3.6) were both purged with high purity nitrogen for 0.5 h. The image was taken 1 h after mixing.

NPs can directly oxidize TMB rather than acting as a catalyst of TMB oxidation by dissolved oxygen.

To verify whether the reaction was initiated by Co^{3+}, Co_3O_4 NPs were treated with acidic $KMnO_4$ and $NaBH_4$, respectively, so the amounts of Co^{3+} or Co^{2+} exposed on the surface of Co_3O_4 NPs were regulated by the strong oxidizing or reducing agents. After removing excess agents by centrifugation and washing the samples thoroughly, they were compared to

dx.doi.org/10.1021/am405009f | ACS Appl. Mater. Interfaces 2014, 6, 1959−1970

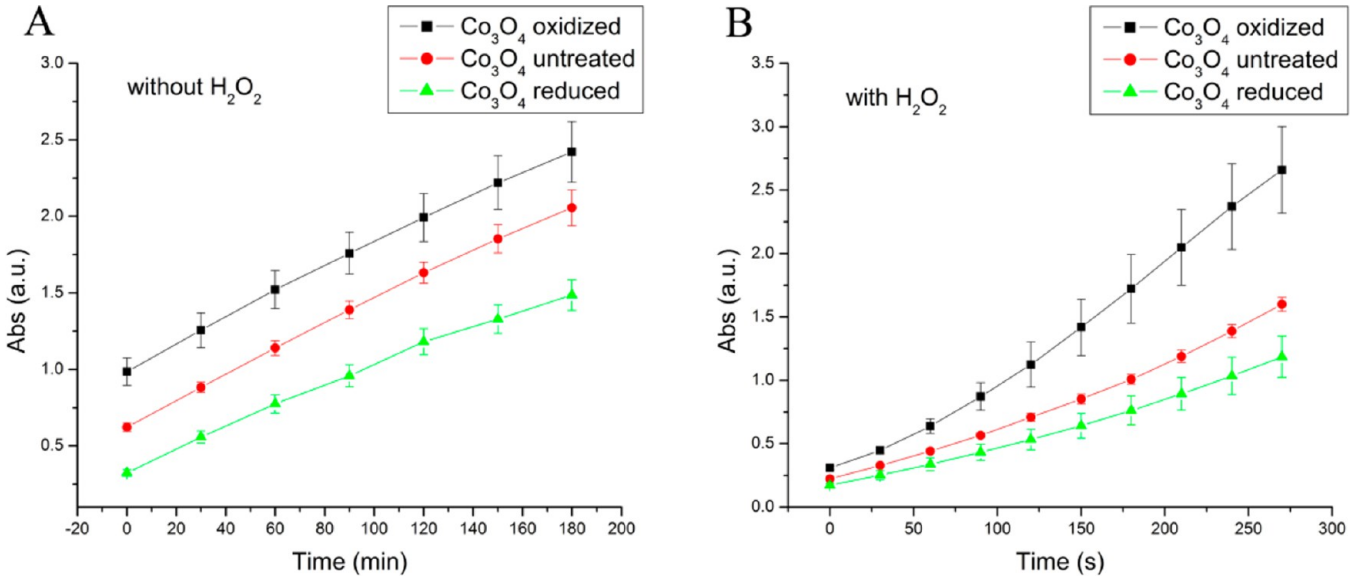

Figure 11. Effect of oxidizing or reducing agent treatment on the activity of Co_3O_4 NPs without H_2O_2 (A) and with H_2O_2 (B). Co_3O_4 NPs were first treated with 0.05 M acidic $KMnO_4$ and 0.05 M $NaBH_4$, respectively, for 30 min. For A, the sample solution contained 0.2 M buffer (pH 3.6) and 0.4 mg/mL TMB with 4 μg/mL Co_3O_4 NPs (treated or untreated). Absorbance data were recorded every 30 min. For B, the sample solution contained 0.2 M buffer (pH 3.6), 0.4 mg/mL TMB, and 0.4 μg/mL Co_3O_4 NPs (treated or untreated) with 1.3 M H_2O_2. Absorbance data were recorded every 30 s. The error bars represent the standard deviation of three measurements.

Scheme 3. Immunohistochemistry Detection Process Based on the Peroxidase-like Activity of Co_3O_4 NPs

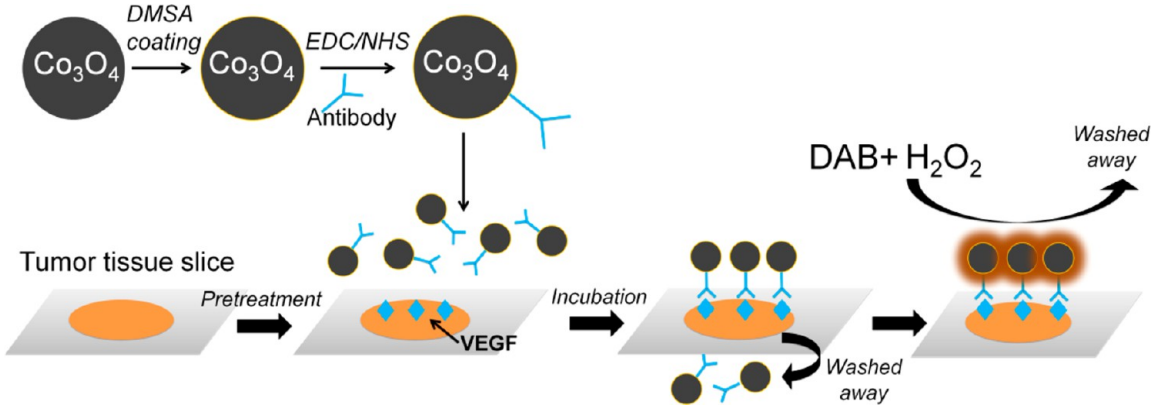

untreated Co_3O_4 NPs using a TMB color reaction. Co_3O_4 NPs treated with acidic $KMnO_4$ showed a higher ability to oxidize TMB, while those treated with $NaBH_4$ showed a lower ability to do this (Figure 11). Acidic $KMnO_4$ can oxidize Co^{2+} into $Co^{3+}$and increase the amount of Co^{3+}. $NaBH_4$ can reduce Co^{3+} into Co^{2+} and can decrease the amount of Co^{3+}. The oxidizability went well with the amount of Co^{3+} and showed that Co^{3+} plays the leading role in the reaction. The comparison between Co_3O_4 NPs and Co^{2+} ions of the same Co content also showed that Co^{2+} ions catalyzed TMB oxidation very inefficiently, so the activity of Co_3O_4 NPs can't come from Co^{2+} (Supporting Information Figure S5). In the Fenton reaction, Fe^{2+} is reported to be the active site, since it can enhance radical generation.[4,40] This distinction confirmed again that Co_3O_4 NPs don't follow the Fenton reaction in an acidic buffer.

3.4. Evaluation of Ab-Co_3O_4 Conjugates. The avastin antibody was immobilized onto the surface of Co_3O_4 NPs by EDC/NHS method to obtain stable Ab-Co_3O_4 conjugates. Compared to Co_3O_4 NPs, Ab-Co_3O_4 conjugates had an apparent increase in hydrodynamic size and a decrease in negative zeta-potential (shown in Table 1). Through Co element and protein quantitation, the final Ab-Co_3O_4 conjugate solution contained 15.0 μg of Co and 5.3 μg of antibody per milliliter. The coupling ratio of Co_3O_4 NPs and antibody was calculated by following the formulas:

$$M_{Co_3O_4} = \frac{4}{3}\pi r^3 \cdot \rho_{Co_3O_4} = 1.19 \times 10^{-18} g \quad (13)$$

$$N_{Co_3O_4} = \frac{m_{Co_3O_4}}{M_{Co_3O_4}} = \frac{2.04 \times 10^{-5}}{1.19 \times 10^{-18}} = 1.71 \times 10^{13} \quad (14)$$

$$M_{antibody} = 149 \text{ KDa} \quad (15)$$

$$N_{antibody} = \frac{m_{antibody}}{M_{antibody}} \times N_A = 2.14 \times 10^{13} \quad (16)$$

$$R_{antibody/Co_3O_4} = \frac{N_{antibody}}{N_{Co_3O_4}} = 1.25 \quad (17)$$

dx.doi.org/10.1021/am405009f | ACS Appl. Mater. Interfaces 2014, 6, 1959−1970

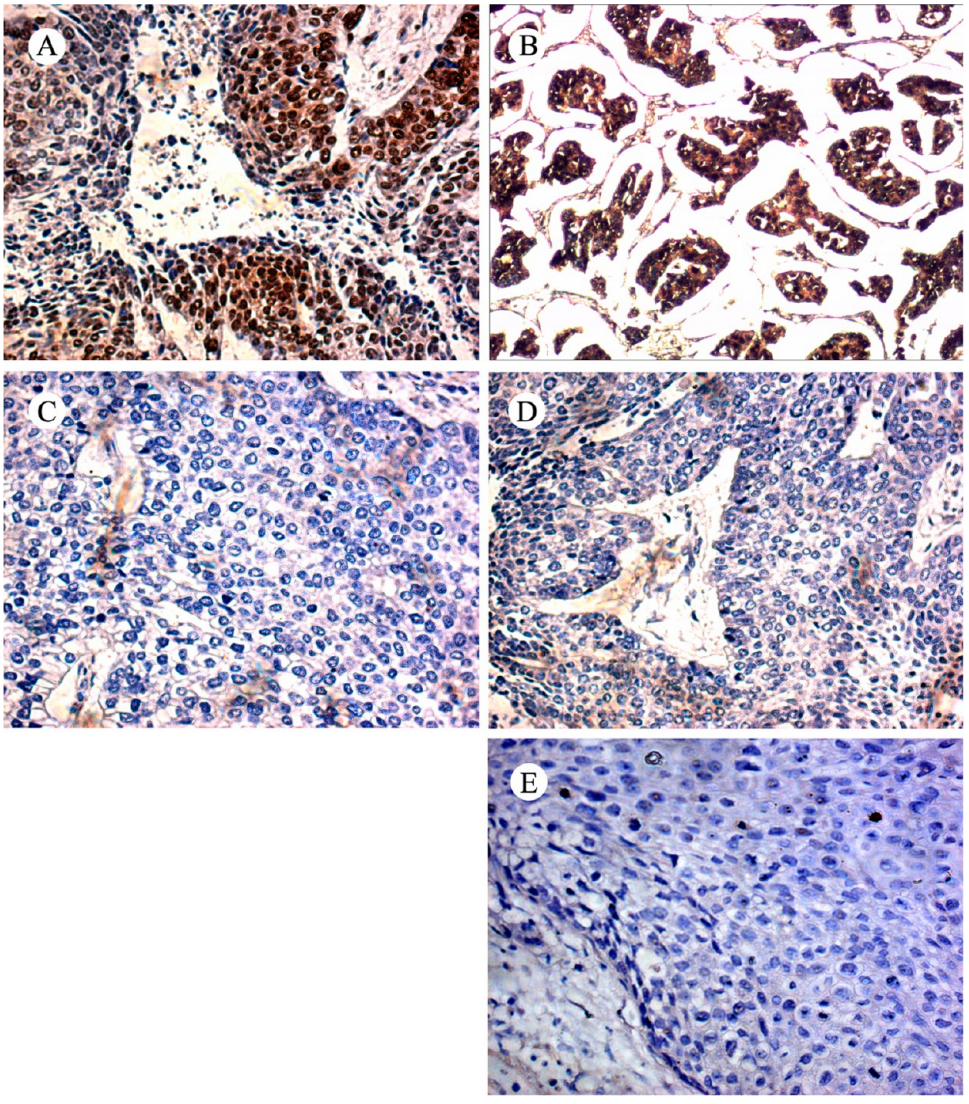

Figure 12. Immunohistochemistry staining images. (A) Incubated with Ab-Co_3O_4 conjugates, (B) stained by natural HRP, (C) incubated with Ab-Co_3O_4 conjugates after avastin blocking, (D) BSA-Co_3O_4 control, and (E) PBS control.

$M_{Co_3O_4}$ and $M_{antibody}$ refer to the masses of single particle and single antibody molecules, respectively. The masses of Co_3O_4 NPs and antibody in 1 mL solution are represented by $m_{Co_3O_4}$ and $m_{antibody}$, which can be calculated from the component analysis results. $N_{Co_3O_4}$ and $N_{antibody}$ refer to the number of particles and antibody molecules, respectively, and r is the average radius of the NPs. The density of Co_3O_4 is $\rho_{Co_3O_4}$. $R_{antibody/Co_3O_4}$ obviously represents the coupling ratio, which means one particle was conjugated with an average of 1.25 antibody molecules.

3.5. Immunohistochemistry Detection with Ab-Co_3O_4 Conjugates. To prove the applicability in bioassay, the Ab-Co_3O_4 conjugates were applied to detect VEGF in tumor tissue slices. VEGF is a signal protein produced by cells that stimulates vasculogenesis and angiogenesis. Because tumors cannot grow beyond a limited size without an adequate blood supply, tumor cells that overexpress VEGF are able to grow and metastasize.[46] Treatment with VEGF as a target has been widely adopted in recent years.[47−49] The avastin antibody is a commercial monoclonal antibody that can specifically bind to VEGF. Tumor tissue slices used in this work were obtained from the Department of Oncology, Zhongda hospital. Homologous slices had confirmed positive VEGF overexpression before the experimental slices were used. The detection process is illustrated in Scheme 3. The avastin antibody immobilized on the surface of a Co_3O_4 nanoparticle can be captured by VEGF on the slice, riveting the conjugates to the antigen area. With the addition of a buffer containing H_2O_2 and DAB, a frequently-used substrate for immunohistochemistry detection, Co_3O_4 then acts as a peroxidase, oxidizing DAB into brown products and depositing them on the surface of the slice.

The immunohistochemical staining results are shown in Figure 12. In tissues treated with Ab-Co_3O_4 conjugates, there was distinct area of brown color where cell nucleii were relatively large and stained dark blue by hematoxylin (shown in Figure 12A). Our Ab-Co_3O_4 conjugates showed comparable labeling function with natural HRP (shown in Figure 12B). The competitive inhibition experiment showed that free antibody addition reduced staining significantly (Figure 12C), proving that binding between the Ab-Co_3O_4 conjugates and the slices relied mostly on the combination of antigen−antibody rather

than non-specific adsorption. No obvious dye was observed in the BSA-Co_3O_4 slices (Figure 12D) and the PBS control (Figure 12E). These results indicate that Co_3O_4 NPs can be used as an excellent enzyme label, due to their high catalytic activity.

CONCLUSIONS

This work investigated the pH-dependent multi-enzyme activities of Co_3O_4 NPs. In alkaline and neutral conditions, Co_3O_4 NPs can catalyze the rapid decomposition of H_2O_2 and superoxide, demonstrating that Co_3O_4 NPs can act as catalase and SOD mimetics. In acidic conditions, Co_3O_4 NPs can catalyze H_2O_2 oxidizing substrate and showed mainly peroxidase-like activity. By employing Co_3O_4 NPs as enzyme mimetics, higher catalytic activities were obtained compared to analogous Fe_3O_4 NPs. The mechanism was analyzed using the ESR method and other verification experiments.

Unlike Fe_3O_4 NPs, Co_3O_4 NPs didn't follow the Fenton reaction and Co^{3+} was confirmed as the leading player in the catalytic reaction. The high redox potential of Co^{3+}/Co^{2+} explains the difference between both the catalytic activity and the mechanism in Co_3O_4 and Fe_3O_4. An immunohistochemical assay based on the peroxidase-like activity of Co_3O_4 NPs proved clearly that Co_3O_4 NPs can be used as potential enzyme labels in place of natural enzymes.

Our work provides a detailed analysis of the reaction mechanism of Co_3O_4 NPs with H_2O_2 in different conditions. The approaches developed here may also help to exploit better enzyme mimetics as tools for biocatalysis and bioassays.

ASSOCIATED CONTENT

Supporting Information

pH dependence of catalytic activity of Co_3O_4 NPs, catalase-like activity of Co_3O_4 NPs in acidic and alkaline conditions, Lineweaver-Burk (double-reciprocal) plots of Fe_3O_4 and Co_3O_4 NPs with TMB or H_2O_2, hydroxyl radical scavenging activity of Co_3O_4 NPs, and comparison of peroxidase-like activity between Co_3O_4 NPs and Co^{2+} ions. This material is available free of charge via the Internet at http://pubs.acs.org.

AUTHOR INFORMATION

Corresponding Author

*E-mail: zhangyu@seu.edu.cn. Tel.: +86 025-83272476. Fax: +86 025-83792460.

Notes

The authors declare no competing financial interest.

ACKNOWLEDGMENTS

We would like to thank Barbara Berman for editorial assistance. This research was supported by the National Basic Research Program of China (No. 2011CB933503, 2013CB733800), the National Natural Science Foundation of China (No. 31170959, 61127002), the Basic Research Program of Jiangsu Province (Natural Science Foundation, No. BK2011036), the Research Fund for the Doctoral Program of Higher Education of China (20110092110029), and the National Key Technology Research and Development Program of China (2012BAI23B02). It was also partially supported by a regulatory science grant under the FDA Nanotechnology CORES Program and by the Office of Cosmetics and Colors, CFSAN/FDA (W.H. and J.Y.). This article is not an official U.S. Food and Drug Administration (FDA) guidance or policy statement. No official support or endorsement by the U.S. FDA is intended or should be inferred.

REFERENCES

(1) Perez, J. M. *Nat. Nanotechnol.* **2007**, *2*, 535−536.
(2) Zhang, L.; Zhang, Q.; Li, J. *Adv. Funct. Mater.* **2007**, *17*, 1958−1965.
(3) Banholzer, M. J.; Millstone, J. E.; Qin, L.; Mirkin, C. A. *Chem. Soc. Rev.* **2008**, *37*, 885−897.
(4) Gao, L. Z.; Zhuang, J.; Nie, L.; Zhang, J. B.; Zhang, Y.; Gu, N.; Wang, T. H.; Feng, J.; Yang, D. L.; Perrett, S.; et al. *Nat. Nanotechnol* **2007**, *2*, 577−583.
(5) Peng, F. F.; Zhang, Y.; Gu, N. *Chin. Chem. Lett.* **2008**, *19*, 730−733.
(6) Yu, F.; Huang, Y.; Cole, A. J.; Yang, V. C. *Biomaterials* **2009**, *30*, 4716−4722.
(7) Zhang, X. Q.; Gong, S. W.; Zhang, Y.; Yang, T.; Wang, C. Y.; Gu, N. *J. Mater. Chem.* **2010**, *20*, 5110−5116.
(8) Liu, S.; Lu, F.; Xing, R.; Zhu, J. J. *Chem.—Eur. J.* **2011**, *17*, 620−625.
(9) Smirnov, A. I.; Voinov, M. A.; Pagan, J. O. S.; Morrison, E.; Smirnova, T. I. *J. Am. Chem. Soc.* **2011**, *133*, 35−41.
(10) Fenton, H. J. H. *J. Chem. Soc.* **1894**, *6*, 899.
(11) Kadiiska, M. B.; Maples, K. R.; Mason, R. P. *Arch. Biochem. Biophys.* **1989**, *275*, 98−111.
(12) Hanna, P. M.; Kadiiska, M. B.; Mason, R. P. *Chem. Res. Toxicol.* **1992**, *5*, 109−115.
(13) Leonard, S.; Gannett, P. M.; Rojanasakul, Y.; Berry, D. S.; Castranova, V.; Vallyathan, V.; Shi, X. *J. Inorg. Biochem.* **1998**, *70*, 239−244.
(14) Strlič, M.; Kolar, J.; Šelih, V. S.; Kočar, D.; Pihlar, B. *Acta Chim. Slov.* **2003**, *50*, 619−632.
(15) Verma, P.; Baldrian, P.; Nerud, F. *Chemosphere* **2003**, *50*, 975−979.
(16) Ou, B.; Woodill, M. H.; Flanagan, J.; Deemer, E. K.; Prior, R. L.; Huang, D. *J. Agric. Food Chem.* **2002**, *50*, 2772−2777.
(17) Feng, J.; Zeng, H. C. *Chem. Mater.* **2003**, *15*, 2829−2835.
(18) Wang, X.; Wu, X. L.; Guo, Y. G.; Zhong, Y.; Cao, X.; Ma, Y.; Yao, J. *Adv. Funct. Mater.* **2010**, *20*, 1680−1686.
(19) Li, Y.; Tan, B.; Wu, Y. *Nano Lett.* **2008**, *8*, 265−270.
(20) Lou, X. W.; Deng, D.; Lee, J. Y.; Feng, J.; Archer, L. A. *Adv. Mater.* **2008**, *20*, 258−262.
(21) Li, W. Y.; Xu, L. N.; Chen, J. *Adv. Funct. Mater.* **2005**, *15*, 851−857.
(22) Li, L.; Chu, Y.; Liu, Y.; Song, J.; Wang, D.; Du, X. *Mater. Lett.* **2008**, *62*, 1507−1510.
(23) Xie, X.; Li, Y.; Liu, Z. Q.; Haruta, M.; Shen, W. *Nature* **2009**, *458*, 746−749.
(24) Hu, L.; Peng, Q.; Li, Y. *J. Am. Chem. Soc.* **2008**, *130*, 16136−16137.
(25) Mu, J.; Wang, Y.; Zhao, M.; Zhang, L. *Chem. Commun.* **2012**, *48*, 2540−2542.
(26) Dong, Y.; He, K.; Yin, L.; Zhang, A. *Nanotechnology* **2007**, *18*, 435602.
(27) Wu, Y.; Song, M.; Xin, Z.; Zhang, X.; Zhang, Y.; Wang, C.; Li, S.; Gu, N. *Nanotechnology* **2011**, *22*, 225703.
(28) Zhao, H. T.; Joseph, J.; Zhang, H.; Karoui, H.; Kalyanaraman, B. *Free Radical Biol. Med.* **2001**, *3*, 599−606.
(29) Kiss, E. *Anal. Chim. Acta* **1973**, *66*, 385−396.
(30) Karen, J.; Robert, W.; Fitzpatrick, J. D. *Anal. Biochem.* **1988**, *175*, 231−237.
(31) Kim, H.; Seo, D. H.; Kim, H.; Park, I.; Hong, J.; Park, K. Y.; Kang, K. *Chem. Mater.* **2012**, *24*, 720−725.
(32) He, W.; Liu, Y.; Yuan, J.; Yin, J. J.; Wu, X.; Hu, X.; Zhang, K.; Liu, J.; Chen, C.; Ji, Y.; Guo, Y. *Biomaterials* **2011**, *32*, 1139−1147.
(33) Deng, H.; Shen, W.; Peng, Y.; Chen, X.; Yi, G.; Gao, Z. *Chem.—Eur. J.* **2012**, *18*, 8906−8911.

(34) Fan, J.; Yin, J. J.; Ning, B.; Wu, X.; Hu, Y.; Ferrari, M.; Andersone, G. J.; Wei, J.; Zhao, Y.; Nie, G. *Biomaterials* **2011**, *32*, 1611−1618.
(35) Klem, M. T.; Resnick, D. A.; Gilmore, K.; Young, M.; Idzerda, Y. U.; Douglas, T. *J. Am. Chem. Soc.* **2007**, *129*, 197−201.
(36) Liebman, J. F.; Vechten, D. V.; Donnelly, K. D.; Fristad, W. E. *Inorg. Chim. Acta* **1986**, *115*, 37−50.
(37) Stolze, K.; Udilova, N.; Nohl, H. *Free Radical Biol. Med.* **2000**, *29*, 1005−1014.
(38) Zhao, H.; Joseph, J.; Zhang, H.; Karoui, H.; Kalyanaraman, B. *Free Radical Biol. Med.* **2001**, *31*, 599−606.
(39) Karaseva, E. I.; Losev, Y.P.; Metelitsa, D. I. *Russ. J. Bioorg. Chem.* **2002**, *28*, 128−135.
(40) Chen, Z.; Yin, J. J.; Zhou, Y. T.; Zhang, Y.; Song, L.; Song, M.; Hu, S.; Gu, N. *ACS Nano* **2012**, *6*, 4001−4012.
(41) Eberhardt, M. K.; Santos, C.; Soto, M. A. *Biochim. Biophys. Acta, Gen. Subj.* **1993**, *1157*, 102−106.
(42) Jonsson, M.; Lind, J.; Reitberger, T.; Eriksen, T. E. *J. Phys. Chem.* **1993**, *97*, 11278−11282.
(43) Shinde, S. S.; Maroz, A.; Hay, M. P.; Anderson, R. F. *J. Am. Chem. Soc.* **2009**, *131*, 5203−5207.
(44) Li, W.; Xu, L.; Chen, J. *Adv. Funct. Mater.* **2005**, *15*, 851−857.
(45) Mate, V. R.; Shirai, M.; Rode, C. V. *Catal. Commun.* **2013**, *33*, 66−69.
(46) Ferrara, N. *Endocr. Rev.* **2004**, *25*, 581−611.
(47) Ferrara, N.; Gerber, H. P.; LeCouter, J. *Nat. Med.* **2003**, *9*, 669−676.
(48) Shojaei, F.; Wu, X.; Malik, A. K.; Zhong, C.; Baldwin, M. E.; Schanz, S.; Fuh, G.; Cerber, H. P.; Ferrara, N. *Nat. Biotechnol.* **2007**, *25*, 911−920.
(49) Ferrara, N.; Hillan, K. J.; Novotny, W. *Biochem. Biophys. Res. Commun.* **2005**, *333*, 328−335.